Morphology Control in Block Copolymer Films Using Mixed Solvent Vapors

Kevin W. Gotrik,[†] Adam F. Hannon,[†] Jeong Gon Son,[†,§] Brent Keller,[†] Alfredo Alexander-Katz,[†] and Caroline A. Ross[†,*]

[†]Department of Materials Science and Engineering, Massachusetts Institute of Technology, 77 Massachusetts Avenue, Cambridge, Massachusetts 02139, United States. [§]Present address: Korean Institute of Science and Technology (KIST), Hwarangno 14-gil 5, Seongbuk-gu, Seoul 136-791, Republic of Korea.

ABSTRACT

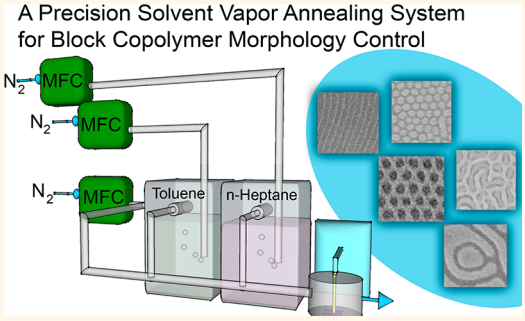

Solvent vapor annealing of block copolymer thin films can produce a range of morphologies different from the equilibrium bulk morphology. By systematically varying the flow rate of two different solvent vapors (toluene and *n*-heptane) and an inert gas, phase maps showing the morphology *versus* vapor pressure of the solvents were constructed for 45 kg/mol polystyrene-*block*-polydimethylsiloxane diblock copolymer films of different thicknesses. The final morphology was correlated with the swelling of the block copolymer and homopolymer films and the solvent vapor annealing conditions. Self-consistent field theory is used to model the effects of solvent swelling. These results provide a framework for predicting the range of morphologies available under different solvent vapor conditions, which is important in lithographic applications where precise control of morphology and critical dimensions are essential.

KEYWORDS: self-assembly · solvent vapor annealing · ps-pdms · block copolymer · toluene · heptane · self-consistent field theory

The self-assembly of block copolymer (BCP) thin films has become increasingly important as a method for nanoscale patterning as the resolution limits of optical lithography are approached.[1−4] BCPs offer a bottom-up approach to nanolithography that is able to reach feature sizes of ∼5 nm and above, surpassing the resolution obtainable by conventional photolithography at lower cost than electron beam lithography. From a technological standpoint, the self-assembly of diblock copolymers presents a high-throughput method for making a variety of 2D periodic or complex patterns consisting of lines and dots from the self-assembly of cylindrical, spherical, or lamellar microdomains.[5] The equilibrium morphology, periodicity, critical dimension size, interfacial width, and diffusivity depend on the Flory−Huggins interaction parameter (χ), the degree of polymerization, N, and the volume fraction f of each block.[5−7]

Microphase separation and/or significant reordering or morphology changes of microdomains can be achieved using thermal annealing, in which the temperature is raised to just below the order−disorder temperature (ODT) in order to improve diffusivity.[8,9] The resulting microdomain morphology and orientation can be manipulated to some extent by altering the BCP film thickness[10] or substrate chemistry. Polystyrene-*block*-poly(methyl methacrylate) (PS-PMMA) is an exemplary BCP for nanolithography with an ODT of 200 °C for a molecular weight of 29 kg/mol and volume fraction 0.5,[2,11] and readily forms microdomains oriented perpendicular to the film plane because PS and PMMA have similar surface energies at the annealing temperature.[1,2] However, its relatively low χ value (∼0.06 at room temperature)[12] limits the minimum microdomain period in this block copolymer system and therefore the minimum feature size. Higher χ BCP systems allow for smaller feature sizes but the theoretical ODT is often well above the polymer's degradation temperature making thermal annealing less practical. For example, if the aforementioned 29 kg/mol block copolymer had a χ of 0.27, the theoretical ODT would exceed 10 000 °C, well above the degradation temperature of ∼450 °C.[13,14]

In contrast, solvent vapor annealing (SVA)[15−27] can be carried out at ambient temperatures. It improves the kinetics of self-assembly by plasticizing the polymer with the incorporation of solvent molecules.

* Address correspondence to caross@mit.edu.

Received for review June 14, 2012 and accepted August 28, 2012.

Published online August 28, 2012
10.1021/nn302641z

This increases the free volume available for polymer diffusion and decreases the glass transition temperature, T_g.[28] The choice of solvent(s) for SVA is based to first order on consideration of the relative Hildebrand solubility parameters, δ. For nonpolar materials the solubility parameter is a good indicator of solubility; in particular, a polymer and a solvent are typically miscible when $|\delta_{poly} - \delta_{solve}| < 2.5$ [MPa]$^{1/2}$.[29] The chain conformation and flexibility also affect the energy required to unwind polymer−polymer segmental contacts and therefore the amount of solvent that a given polymer will absorb.[30] The amount of solvent incorporation during exposure to the solvent vapor can be tracked *in situ* by measuring film swelling using a number of optical spectroscopy techniques.[31]

Exposure to a solvent vapor has several effects on the BCP, including an increase in volume and diffusivity, a decrease in the effective χ proportional to the amount of solvent present at the interface between the blocks,[32,33] a change in relative surface energies of the blocks at the vapor−BCP interface, and a change in the effective *f* dependent on the swelling of each block by the solvent. SVA has the added advantage of reversibility, in which the microdomain morphology can be changed repeatedly by changing the solvent vapor conditions.[23,34] SVA therefore enables tuning of the periodicity and the morphology over a wide range,[23,35−37] and by modifying the surface energy of the film/air interface, SVA can mitigate preferential wetting by one block which favors in-plane microdomain orientations. This is particularly important in high-χ BCPs which have greater differences between the surface energies of the blocks, making it more difficult to form the perpendicularly oriented microdomains desirable for nanolithography.

SVA has often been carried out using a simple experimental system in which thin BCP films are placed in a chamber which also contains a reservoir of liquid solvent(s), whose evaporation provides an atmosphere of solvent vapor.[36] This technique has been used to demonstrate tunability of the morphology in polystyrene-*block*-polydimethylsiloxane (PS-PDMS, $\chi = 0.27$) in a vapor produced from a liquid mixture of toluene and heptane,[23] and even greater tunability of higher-χ poly(2-vinylpyridine)-*block*-polydimethylsiloxane in a variety of solvents.[38] However, in the reservoir system it is difficult to independently control the partial vapor pressures of the solvents. In contrast, continuous flow systems provide simultaneous flow, mixing, and reactions of flowing species,[39,40] and have been used for solvent annealing by exposing the sample to a saturated vapor stream produced by bubbling inert gas through a liquid solvent. This enables control over the vapor concentration[10,41] and has been used to investigate solvent vapor pressure and deswelling rate effects on microdomain morphology and orientation, for example, using a combinatorial microfluidic approach.[15] Vapor pressures can be varied by diluting the solvent vapor using a separate stream of N_2.[22,42] However, a systematic investigation of the morphological effects of independent control of the vapor pressures of two different solvents on a BCP film has not been presented.

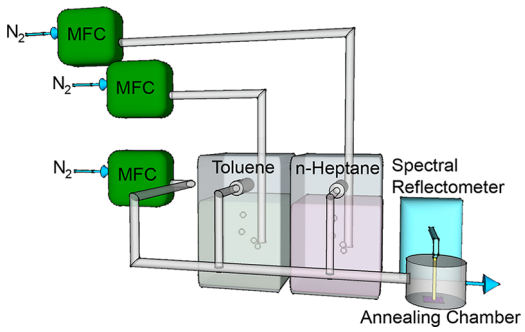

Figure 1. Thin films of PS, PS-PDMS, and PDMS are spin-cast onto Si. These films are annealed in a chamber into which saturated vapor streams are introduced and the film swelling is tracked *in situ*.

In this study we demonstrate the effects of varying the flow rates of two different solvent vapors and a diluent gas on the microphase separation of a BCP film by showing how the morphology of the microdomains can be mapped as a function of vapor pressure and swelling ratio, and compare the results to those obtained on the same BCP annealed using a solvent reservoir. This provides a general framework for understanding the SVA process and for designing processing conditions that allow specific morphologies to be achieved in a BCP film.

RESULTS AND DISCUSSION

A 45.5 kg/mol (number average molecular weight) PS-PDMS (Polymer Source, Inc. P7517-SDMS, $f_{pdms} = 0.32$) BCP which forms a bulk cylindrical morphology with a domain spacing, L_0, of approximately 35 nm was used in this study. Homopolymers of 1390 kg/mol PDMS (100 000 cSt Dow Corning 200 fluid) and 1350 kg/mol PS (Polymer Source, Inc. P620-S) were prepared as thin films for comparison. High molecular weights of the homopolymers were used to retard dewetting, because low molecular weight (<15 kg/mol) PS and PDMS dewetted at room temperature in minutes. The SVA system is shown in Figure 1 and includes three independently controlled vapor streams of saturated toluene, saturated heptane, and nitrogen. This differs from the reservoir system used in previous work on the same BCP and solvents where liquid mixtures of solvents were placed in a chamber with a small leak.[23] Relevant solubility parameters are given in Table 1.

Thin films of the PS, PDMS, and PS-PDMS were spin-cast onto Si substrates as described in the Methods section. For the BCP films, the substrate was coated with a PDMS brush to improve self-assembly kinetics.

TABLE 1. Solubility Parameters of the Solvents and Polymers Investigated.[29]

material	solubility parameter ($MPa^{1/2}$)
heptane	15.3
PDMS	15.5
PS	18.5
toluene	18.3

The samples were annealed under a range of vapor pressures while the film swelling was monitored *in situ* by spectral reflectometry. The vapor pressures in the chamber reached steady state after 15 min as measured from the changes in magnitude of the absorption peaks of toluene[43] in the UV region with the spectral reflectometer, and the films were annealed for 1 h at room temperature (25 ± 1 °C). Microphase separation was complete by at most 30 min (shorter times were not examined) but the correlation length of the microdomain array increased if the annealing time was raised to 1 h. The films were quenched by exposure to a burst of N_2 which removed most of the solvent and deswelled the films within 1 s, according to the color change of the film. The BCP thin films were then reactive-ion etched to remove the surface layer of PDMS and then the PS matrix to reveal the underlying morphology of oxidized PDMS microdomains.

Considering the low flow rates of the solvent (<10 sccm), the high solvent evaporation rates, and the large cross-sectional area of the bubbler (>100 cm^2), we assume that each bubbler delivers solvent vapor at its room temperature saturated vapor pressure, $p^*_{tol} = 22$ Torr for toluene and $p^*_{hep} = 40$ Torr for heptane. As shown in the Supporting Information (SI) the partial pressure of solvent *i* in the chamber is approximated by

$$p_i = p_i^* \left(\frac{q_i}{q_{tol} + q_{hep} + q_{N_2}} \right) \quad (1)$$

where *q* (mol/min) represents the total molar flow rate of the solvent plus N_2 from the bubbler. Calculations of these partial pressures are plotted as solid blue lines in Figure 2 for the case that $q_{tol} + q_{hep} = 10$ sccm while q_{N_2} is allowed to vary from 0 to 20 sccm.

The dashed line shows the vapor pressure above a mixture of liquid toluene plus heptane at room temperature, which approximates the partial pressures available from a solvent anneal process using a liquid reservoir. The toluene/heptane mixture is moderately nonideal,[44] and is described by the nonrandom two-liquid (NRTL) model, in which the activity coefficient (γ) of a solvent in a binary mixture is given by

$$\ln \gamma_1 = x_2^2 \left[\frac{\tau_{12}\, e^{-\alpha_{12}\tau_{12}}}{(x_2 + x_1\, e^{-\alpha_{12}\tau_{12}})^2} + \frac{\tau_{21}\, e^{-2\alpha_{12}\tau_{21}}}{(x_1 + x_2\, e^{-\alpha_{12}\tau_{21}})^2} \right] \quad (2)$$

where (1,2) are the two solvents (toluene, heptane), *x* is the molar fraction in the liquid, and the coefficients α and τ are determined experimentally.[45] The coefficients for mixtures of toluene/heptane are listed in the SI. The partial pressure of solvent *i* is then given by $p_i = \gamma_i x_i p_i^*$. The resulting partial pressures are actually higher than those achieved from the mixing of saturated vapor flows in the annealing chamber of Figure 1. While the reservoir system can access these high partial pressures, the mixed-flow system is capable of reaching much lower partial pressures of solvents, which is important for annealing lower-molecular weight BCPs.

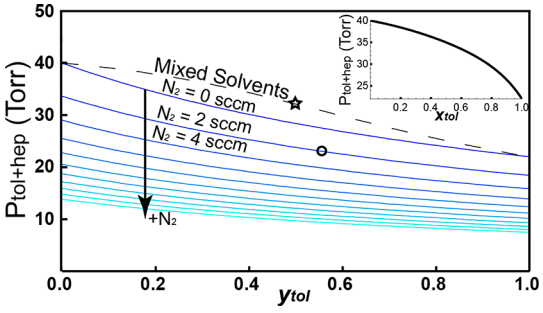

Figure 2. The range of cosolvent vapor conditions achievable in the solvent anneal process. The total partial pressure of toluene and heptane is plotted against y_{tol}, the molar fraction of toluene in the toluene plus heptane solvent vapor phase. The solid lines show the conditions achievable with two separate solvent flows ranging from 0 to 10 sccm with incorporation of various additional amounts of N_2. Circle: Example of a condition resulting from 7/3/2 sccm of tol/hep/N_2. The dashed line indicates the vapor pressure conditions available in proximity to a reservoir containing a mixed cosolvent liquid solution at room temperature. Star: Example of condition resulting from a cosolvent mixture where the molar fraction of toluene in the liquid $x_{tol} = 0.67$. Inset: The relation between total solvent vapor pressure and the fraction of toluene in the liquid phase for a reservoir of mixed solvent, showing a positive deviation from ideality.

In homopolymer/solvent systems the film swelling, given by D/D_0 where *D* is the swollen film thickness and D_0 is the initial thickness, is related to the partial pressure of a solvent and the solvent−polymer interaction parameter χ_{sp} according to[31]

$$\ln\left[\frac{p}{p^*}\right] = \chi_{sp}\left(\frac{D_0}{D}\right)^2 + \ln\left[1 - \frac{D_0}{D}\right] + \left(1 - \frac{1}{N}\right)\frac{D_0}{D} \quad (3)$$

where *N* is the degree of polymerization. This predicts the highest swelling at the saturated partial pressures, but the swelling ratios drop as the partial pressures decrease.

Figure 3a gives an example of the swelling of the BCP and the two homopolymer films after 1 h for the case of no N_2 flow, with various flow rates of toluene and heptane vapors, where y_{tol} is the molar fraction of toluene in the toluene plus heptane vapor. Figure 3b shows the predicted partial pressures of the solvent vapors under these conditions. At high heptane vapor pressure, the PDMS swelling ratio (D/D_0) approached 3 while the PS incorporated very little heptane. Toluene,

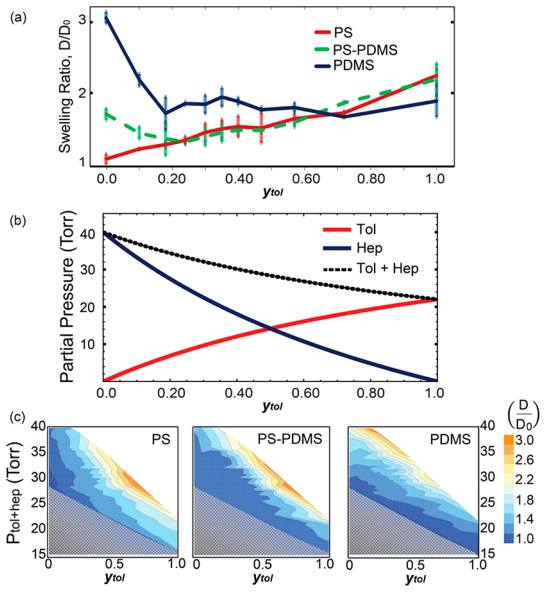

Figure 3. (a) Swelling ratios of PS, PS-PDMS, and PDMS for different flow rates of saturated toluene and heptane vapors with no additional nitrogen diluent (upper horizontal scale). The corresponding mole fraction of toluene in the toluene plus heptane vapor is shown on the nonlinear lower horizontal scale. (b) The expected partial pressures of the solvents based on their flow ratios into the solvent vapor annealing chamber with no additional N_2 flow. (c) Contour plots of the swelling exhibited by the PS, PS-PDMS, and PDMS films under different vapor pressure conditions achievable by the controlled flow system and the mixed solvent solution reservoir system. The shaded regions at the bottom left resulted in very little swelling and morphologies were not investigated.

however, exhibited less selectivity between PS and PDMS, which swelled by a factor of 2.2 and 1.8 respectively. Although toluene would be expected to swell PDMS very little based on the solubility parameters, the very low T_g and high chain flexibility of PDMS allows for a significant amount of toluene incorporation. The swelling ratio of the BCP was intermediate to that of the homopolymers, but was closer to that of PS, the majority block.

Figure 3c shows the swelling ratios of the BCP and the homopolymers over the full range of toluene and heptane partial pressures available at room temperature from the continuous flow system, combined with data from annealing in a chamber containing a reservoir of mixed solvents. The two sets of data show consistent trends. Swelling increased with partial pressure, as expected, and showed a maximum for toluene fraction $y_{tol} < 0.2$ for the PDMS, and $y_{tol} \approx 0.7$ for the PS and the BCP. The swelling ratios of the polymer films at the upper limit of the vapor pressures achievable with the continuous vapor flow system (*i.e.*, with no diluting N_2 flow) were less than those achievable from the reservoir system for a given $0 < y_{tol} < 1$, as expected from the nonideality of the liquid mixture.

After annealing, the BCP films were etched to reveal the PDMS microdomain morphology, and a representative selection of images is shown in Figure 4a–i for initial film thicknesses of $D_0 \approx L_0$ and $1.5L_0$. The microdomain morphologies are summarized in Figure 5, showing the regimes of vapor pressures within which each morphology formed.

In the high vapor pressure regime, films of initial thickness close to L_0 (38 nm) showed a transition from discontinuous in-plane lamellae (with lateral dimensions up to around 10 μm) to perforated lamellae to in-plane cylinders of decreasing width and period as y_{tol} increased. The morphology control between perforated lamellae and cylinders was observed previously in samples processed using a reservoir of mixed liquid solvents.[23] However, the lower vapor pressures in the continuous flow system were also able to produce micelles and disordered structures not obtainable from the reservoir anneal. A significant overlap existed between some of the morphologies, especially between in-plane cylinders and lamellae, which formed together on the same substrate.

The thicker films, $1.5L_0$, showed several qualitative differences. Cylinders were formed over a wider range of vapor pressures, lamellae formed less readily, and the perforated lamellar morphology was suppressed. A bicontinuous morphology (Figure 4f) and a two-phase voided film caused by solvent aggregation within the film and subsequent removal leading to voids (Figure 4h) were found within limited ranges of vapor pressure. In particular, short vertical cylinders of PDMS, Figure 4e, occurred when $y_{tol} > 0.4$ at lower pressures, most likely resulting from a combination of film thickness incommensurability and a reduction in the surface energy difference between the blocks in the solvent atmosphere.[46] Cross sectional images, Figure 4i, confirmed the identification of vertical cylinders with an aspect ratio of ~1.1. Vertical cylinders and in-plane cylinders coexisted at intermediate vapor pressures but the vertical cylinders were suppressed as the partial pressure of toluene and heptane increased. To test whether these vertical cylinder structures had a surface layer of PDMS, another sample of the annealed film was etched omitting the first etch step which removes the PDMS layer. This had no noticeable effect on the observed morphology indicating that there is little or no PDMS surface layer under these annealing conditions, suggesting that the solvent vapor reduces the surface energy difference between the blocks. Additionally, the vertical cylinders of PDMS had good close-packed order with correlation lengths on the order of 500 nm. This is different from the micellar structures seen at low vapor pressures and low y_{tol} which had low correlation length and poor uniformity.

Varying levels of osmotic rupture were observed under conditions of high PDMS swelling and low PS swelling where cylinders of PDMS with interior voids were observed (Figure 4g). Osmotic rupture of PS-PDMS has been reported previously[47] but the process

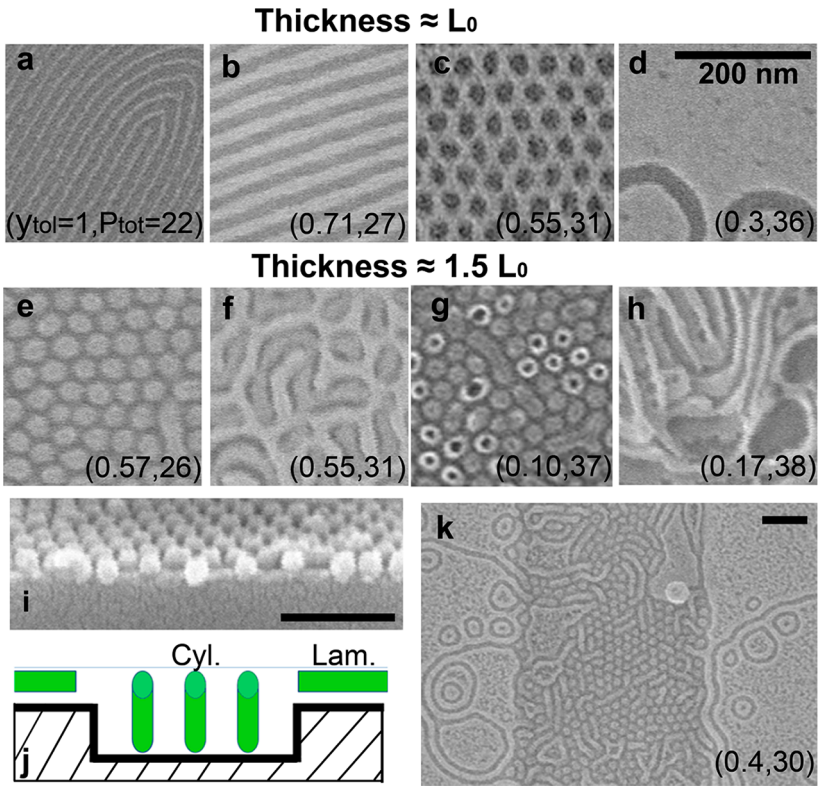

Figure 4. A sampling of morphologies seen in different film thicknesses of $\sim L_0$ and $\sim 1.5L_0$ at different SVA conditions (fraction of toluene in vapor, total vapor pressure (Torr), is labeled on each image): (a,b) in-plane cylinders with different widths; (c) perforated lamella; (d) lamellae of limited width; (e) vertical cylinders; (f) bicontinuous; (g,h) two-phase coexistence of solvent and polymer which results in film voids of varying size upon quenching; (i) cross section of vertical cylinder formation; (j) schematic of self-assembly of a film deposited on a substrate with trenches; (k) experimental results of the experiment shown in image j, with vertical cylinders in the $1.5L_0$ thickness film in the trench and lamellae in the L_0 thickness film on the mesa.

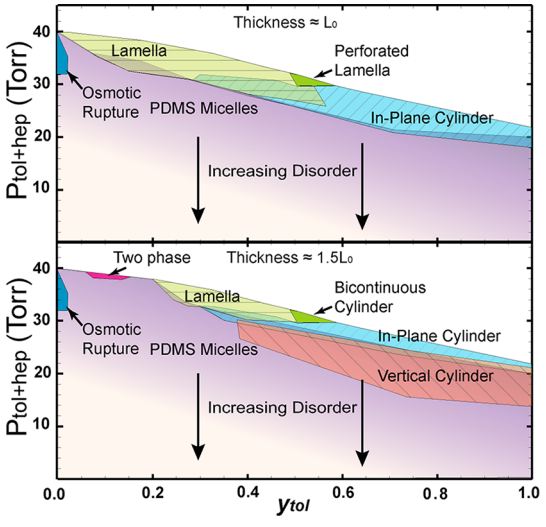

Figure 5. A phase diagram of the morphologies produced by solvent vapor annealing a 45 kg/mol PS-PDMS ($f_{PDMS} = 0.32$) film under different partial pressures of toluene and heptane at room temperature. BCP film thicknesses of $\sim L_0$ (upper panel) and $\sim 1.5\ L_0$ (lower panel) were explored. At low solvent vapor pressures the BCP was kinetically trapped in the PDMS micelle morphology that formed during spin coating, and its ordering (*i.e.*, the correlation length of the micelle array) improved as the vapor pressure increased.

required full submersion of the BCP film in a PDMS-selective solvent. A two-phase region at high heptane pressure was characterized by voids in the film caused by regions of liquid solvent within the BCP that are removed rapidly during the quench (Figure 4h). These results show that the continuous flow system produced a much richer range of microphase-separated structures than the reservoir system, with the perpendicular cylinders being particularly interesting for lithographic applications.

To demonstrate the formation of mixed morphologies, a film was prepared on a substrate with trenches of depth $L_0/2$ such that the thickness was $\sim L_0$ on the mesas and $\sim 1.5L_0$ in the trenches. This was solvent annealed (6:10 sccm flow ratio of Tol:Hep) to produce vertical cylinders with a few in plane cylinders in the trenches, and in-plane lamellae with a few cylinders on the mesas, Figure 4j,k.

Self-consistent field theory (SCFT) simulations were performed in order to model morphology changes during SVA (see SI for details and further discussion of the simulation methodology). The equilibrium morphology of a film of diblock copolymer AB was modeled in the presence of two different solvents S_A and S_B, with S_A fully selective to block A and S_B to B. These simulations used a Langevin dynamics scheme seeded with an initial in-plane cylindrical structure[48,49] to reduce computation time. (The seeding explains why

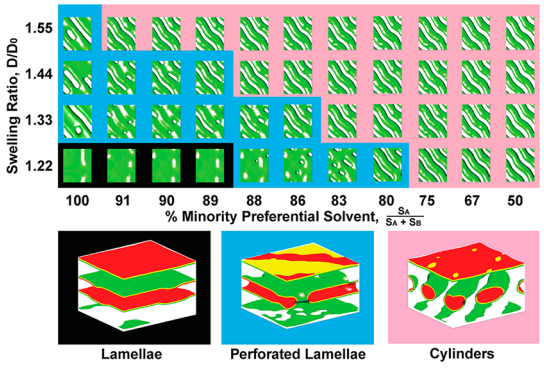

Figure 6. SCFT simulations of a cylinder phase BCP ($f = 0.32$, $\chi N = 18.0$) thin films ($D_0 = 1.7L_0$) with varying volume expansions D/D_0 caused by the incorporation of solvents selective to each block A and B. The images show the isosurface in green at which the density of the minority polymer plus its solvent S_A was $\varphi = 50\%$. In the representative lower 3D images, additional surfaces are shown for $\varphi = 60\%$ (yellow) and 70% (red). The green isosurface is shown as a reflective surface to give an idea of its flatness. In images with a black background, the minority block forms a lamella without any perforations; blue background indicates a perforated lamella or bridged cylinders, and a pink background indicates separated cylinders.

the various simulations of Figure 6 have the same cylinder orientation.) The model used $\chi N = 18.0$ which is less than the χN of ~100 that is expected in the PS-PDMS experimental system (which has $N \approx 485$) at room temperature without solvent incorporation. A lower χN was used because the statistical repeat unit (used in the simulations) is 2.8 times larger than a single experimental chemical monomer at the level of coarse-graining used, and because solvent incorporation is known to reduce the effective χ.[32,33] Solvent incorporation was modeled explicitly through the partitioning of the solvent as a monatomic fluid in addition to the traditional single chain partitioning of the block copolymer and implicitly through the choice of a lower χ value, and swelling evolution was modeled by keeping the overall copolymer volume constant during the addition of solvent volume.

The model showed that the density profile of S_A closely overlapped the density profile of block A, and S_B overlapped B. Within this formalism, toluene, which experimentally showed an almost neutral selectivity between PS and PDMS, would be modeled as a superposition of two different fully selective solvents with fractional amounts determined from the measured incorporation of toluene into each of the blocks.

The results of the simulations are shown in Figure 6. Each simulation bar one (see SI) started with the same initial configuration of in-plane cylinders for $f = 0.32$ in a cell of dimensions $3L_0$ by $2(3)^{1/2}L_0$ (commensurate with cylinders or a hexagonally packed perforated lamella) with periodic boundary conditions, then the simulation cell thickness was increased and the empty volume filled with S_A and S_B, and allowed to equilibrate. The initial thickness D_0 was chosen by simulating a range of film thicknesses to find the range that produced a monolayer of in plane cylinders. Swelling was modeled by increasing the cell thickness sequentially by one grid point, at the level of coarse-graining used. The ratio $S_A/(S_A + S_B)$ was varied from 50% to 100%, where A represents the minority block. The 50% ratio approximates pure toluene assuming toluene to be entirely neutral in its swelling of PS and PDMS, while the 100% ratio approximates annealing in pure heptane. Perforated lamellae were defined as states with a connection between neighboring in-plane cylinders while lamellae occurred when the entire plane of cylinders of minority polymer density connected.

As the solvent became more selective to the minority block, that is, increasing $S_A/(S_A + S_B)$, the morphology transitioned from narrow cylinders to wider cylinders to perforated lamellae and then to lamellae. This agrees qualitatively with the experiment, where the narrow cylinder-wide cylinder-perforated lamella–lamella sequence occurs with increasing heptane (preferential to PDMS). The model also suggests that higher swelling (*i.e.*, higher vapor pressure) for a given $S_A/(S_A + S_B)$ favors cylinders over lamellae, because proportionately more of the minority-selective solvent is required to increase f into the lamellar regime. In agreement, comparing Figure 3b for the BCP and the upper panel of Figure 5, the highest swelling ratios corresponded to cylindrical morphologies. Considering that adding solvent S_A has the effect of increasing f_A, these trends are comparable to other studies relating BCP morphology to f. The agreement between the observed and modeled morphological transitions suggests that the drying of the swollen film was fast enough to preserve the morphology present during the solvent anneal as has been suggested for thin films.[25] The simulation did not generate the perpendicular cylinder morphology, presumably due to the preferential wetting of the top surface by the minority block in the simulation, and because the swelling ratios modeled were smaller than those which generated perpendicular cylinders.

CONCLUSION

Solvent annealing using continuous flows of saturated solvent vapors and an inert gas diluent can access regimes of solvent partial pressure which are not available from a simple solvent anneal system that uses a reservoir of mixed liquid solvents, in which nonidealities in cosolvent mixtures govern the available partial pressures of the solvents. The independent control of vapor pressures in the continuous flow system provides a powerful and general method for mapping the swelling ratio and morphology as a function of the partial pressures of the solvents, and provides access to a wide variety of morphologies from a block copolymer. For example, perpendicular cylinders were demonstrated in 45 kg/mol PS-*b*-PDMS

which are inaccessible from a reservoir anneal. Further, a continuous flow system can provide low vapor pressures of solvent which are necessary for microphase separation in low molecular weight BCPs required for small period patterns without dewetting or formation of two-phase structures. Self-consistent field theory modeling of solvent incorporation showed morphological transitions that correspond qualitatively to the experiment. Morphology control, including manipulation of periodicity, critical dimension and geometry, are critical for the application of BCPs to nanolithography, and solvent annealing is a key enabling process step. The continuous flow solvent anneal system can be adapted to include larger numbers of solvent vapor streams, which may be appropriate for triblock terpolymers or other more complex polymers.

METHODS

Thin films of PS-PDMS ($D_o \approx 38$ nm) and PDMS (≈70 nm) were spun-cast onto 1 cm × 1 cm Si wafers that were pretreated with an hydroxyl-terminated PDMS brush layer (0.8 kg/mol, 14 h at 170 °C followed by a toluene rinse) to increase mobility for the BCP and to improve wetting for the PDMS, which is very prone to dewetting due to its low T_g (≈100 °C). PS (≈70 nm) films were spun-cast onto prime Si wafers. The thin films were placed inside the annealing chamber, and their thicknesses were recorded by spectral reflectometer. Because of the film thickness gradients that can occur during spin coating on such small samples, only the most uniform areas of the center region of each sample was considered for this analysis. Different combinations of flow rates for each of the solvent lines and for the N_2 dilution line were swept. These flow rates resulted in the annealing chamber reaching steady state after 15 min. After 1 h, the reflectometer was rebaselined to take into account the presence of solvents which added absorption peaks in the UV (see SI) and then the polymer film thicknesses were recorded. The BCP thin films reached their steady state equilibrium morphology after approximately 30 min, with longer annealing time effective in improving microdomain size and orientation. The BCP thin films were then reactive-ion etched by 5 s of CF_4 (10 mTorr, 90 W) and 22 s of O_2 (10 mTorr, 90 W) to remove the PS matrix and the PDMS surface layer to reveal the underlying oxidized PDMS morphology.

For the solvent vapor annealing, a N_2 (Airgas, Inc., 99.9997% purity) backpressure of 200 kPa was distributed to three high precision mass flow controllers (MKS Inc., M100B) which were rated to control flow rate to within 1% of the set point and had a total range of 0−10 sccm. Two of the flow lines were sent through custom glass solvent bubblers that contained toluene and heptane (VWR, >99.9%) at rates of 0−10 sccm. These solvent chambers were placed after the MFCs, to avoid solvent degradation of the MFCs. The solvent flow passed through $^1/_4$ in. OD fluorinated ethylene propylene (FEP) tubing which shows high resistance to toluene/heptane absorption and then passed through small diameter syringes which were joined together before entering the annealing chamber. The syringes were used to sufficiently increase flow rate and decrease possible backflow from one solvent line to another, and a third N_2 flow line was used to control vapor pressure dilution. The annealing chamber (~80 cm^3) consisted of an in and out port and a removable sealed quartz plate which allowed for *in situ* measurements from a spectral reflectometer (Filmetrics, Inc., F20−UV, 250−1500 nm). The quartz plate was tightly sealed by utilizing a perfluoroelastomer O-ring (Markez Inc., Z1210) to minimize interaction with solvent annealing vapors. The solvent annealing was done using liquid solvents held at ambient temperature to minimize the effect of thermal gradients that could occur in the system where the solvent vapor is flowing. These thermal gradients can cause condensation of solvent on the polymer sample unless the polymer sample temperature is at least equal to the solvent temperature. The effects of changing the polymer temperature will be reported separately.

Conflict of Interest: The authors declare no competing financial interest.

Acknowledgment. The authors gratefully acknowledge support of the Semiconductor Research Corporation, the FENA Center, Tokyo Electron, Taiwan Semiconductor Manufacturing Company, and the National Science Foundation.

Supporting Information Available: Additional information on the solvent vapor pressures and nonrandom two-liquid model, additional SEM micrographs, toluene optical absorption, and SCFT modeling. This material is available free of charge *via* the Internet at http://pubs.acs.org.

REFERENCES AND NOTES

1. Kim, S. O.; Solak, H. H.; Stoykovich, M. P.; Ferrier, N. J.; dePablo, J. J.; Nealey, P. F. Epitaxial Self-Assembly of Block Copolymers on Lithographically Defined Nanopatterned Substrates. *Nature* **2003**, *424*, 411–414.
2. Ruiz, R.; Kang, H.; Detcheverry, F. A.; Dobisz, E.; Kercher, D. S.; Albrecht, T. R.; DePablo, J. J.; Nealey, P. F. Density Multiplication and Improved Lithography by Directed Block Copolymer Assembly. *Science* **2008**, *321*, 936–939.
3. Stoykovich, M. P.; Nealey, P. F. Block Copolymers and Conventional Lithography. *Mater. Today* **2006**, *9*, 20–29.
4. Park, S.; Lee, D. H.; Xu, J.; Kim, B.; Hong, S. W.; Jeong, U.; Xu, T.; Russell, T. P. Macroscopic 10-Terabit-per-Square-Inch Arrays from Block Copolymers with Lateral Order. *Science* **2009**, *323*, 1030–1033.
5. Bates, F. S.; Fredrickson, G. H. Block Copolymer Thermodynamics: Theory and Experiment. *Annu. Rev. Phys. Chem.* **1990**, *41*, 525–557.
6. Lodge, T. P.; Dalvi, M. C. Mechanisms of Chain Diffusion in Lamellar Block Copolymers. *Phys. Rev. Lett.* **1995**, *75*, 657–660.
7. Leibler, L. Theory of Microphase Separation in Block Copolymers. *Macromolecules* **1980**, *13*, 1602–1617.
8. Xiao, S.; Yang, X.; Edwards, E. W.; La, Y. H.; Nealey, P. F. Graphoepitaxy of Cylinder-Forming Block Copolymers for Use as Templates to Pattern Magnetic Metal Dot Arrays. *Nanotechnology* **2005**, *16*, S324–S329.
9. Kim, H. C.; Russell, T. P. Ordering in Thin Films of Asymmetric Diblock Copolymers. *J. Polym. Sci., Polym. Phys.* **2001**, *39*, 663–668.
10. Knoll, A.; Magerle, R.; Krausch, G. Phase Behavior in Thin Films of Cylinder-Forming ABA Block Copolymers: Experiments. *J. Chem. Phys.* **2004**, *120*, 1105–1116.
11. Kim, E.; Choi, S.; Guo, R.; Ryu, D. Y.; Hawker, C. J.; Russell, T. P. Transition Behavior of PS-*b*-PMMA Films on the Balanced Interfacial Interactions. *Polymer* **2010**, *51*, 6313–6318.
12. Bucholz, T. L.; Loo, Y. L. Phase Behavior of Near-Monodisperse Semifluorinated Diblock Copolymers by Atom Transfer Radical Polymerization. *Macromolecules* **2006**, *39*, 6075–6080.
13. Russell, T. P.; Hjelm, R. P.; Seeger, P. A. Temperature Dependence of the Interaction Parameter of Polystyrene and Poly(methyl methacrylate). *Macromolecules* **1990**, *23*, 890–893.
14. Yan, H.; Blanford, C. F.; Lytle, J. C.; Carter, C. B.; Smyrl, W. H.; Stein, A. Influence of Processing Conditions on Structures of 3D Ordered Macroporous Metals Prepared by Colloidal Crystal Templating. *Chem. Mater.* **2001**, *13*, 4314–4321.
15. Albert, J. N. L.; Bogart, T. D.; Lewis, R. L.; Beers, K. L.; Fasolka, M. J.; Hutchison, J. B.; Vogt, B. D.; Epps, T. H. Gradient Solvent Vapor Annealing of Block Copolymer Thin Films

Using a Microfluidic Mixing Device. *Nano Lett.* **2011**, *11*, 1351–1357.
16. Cavicchi, K. A.; Berthiaume, K. J.; Russell, T. P. Solvent Annealing Thin Films of Poly(Isoprene-*b*-Lactide). *Polymer* **2005**, *46*, 11635–11639.
17. Peng, J.; Kim, D. H.; Knoll, W.; Xuan, Y.; Li, B.; Han, Y. Morphologies in Solvent-Annealed Thin Films of Symmetric Diblock Copolymer. *J. Chem. Phys.* **2006**, *125*, 647021–647028.
18. Paik, M. Y.; Bosworth, J. K.; Smilges, D. M.; Schwartz, E. L.; Andre, X.; Ober, C. K. Reversible Morphology Control in Block Copolymer Films *via* Solvent Vapor Processing: An *in Situ* GISAXS Study. *Macromolecules* **2010**, *43*, 4253–4260.
19. Di, Z.; Posselt, D.; Smilgies, D. M.; Papadakis, C. M. Structural Rearrangements in a Lamellar Diblock Copolymer Thin Film During Treatment with Saturated Solvent Vapor. *Macromolecules* **2010**, *43*, 418–427.
20. Harant, A. W.; Bowman, C. N. Solvent Vapor Annealed Block Copolymer Films on Organosilane Self-Assembled Monolayers. *J. Vac. Sci. Technol., B* **2005**, *23*, 1615–1621.
21. Xuan, Y.; Peng, J.; Cui, L.; Wang, H.; Li, B.; Han, Y. Morphology Development of Ultrathin Symmetric Diblock Copolymer Film *via* Solvent Vapor Treatment. *Macromolecules* **2004**, *37*, 7301–7307.
22. Tada, Y.; Yoshida, H.; Hirai, T.; Bosworth, J. K.; Dobisz, E.; Ruiz, R.; Takenaka, M.; Hayakawa, T.; Hasegawa, H. Directed Self-Assembly of POSS Containing Block Copolymer on Lithographically Defined Chemical Template with Morphology Control by Solvent Vapor. *Macromolecules* **2012**, *45*, 292–304.
23. Jung, Y. S.; Ross, C. A. Solvent-Vapor-Induced Tunability of Self-Assembled Block Copolymer Patterns. *Adv. Mater.* **2009**, *21*, 2540–2545.
24. Vogelsang, J.; Brazard, J.; Adachi, T.; Bolinger, J. C.; Barbara, P. F. Watching the Annealing Process One Polymer Chain at a Time. *Angew. Chem., Int. Ed.* **2011**, *50*, 2257–2261.
25. Phillip, W. A.; Hillmyer, M. A.; Cussler, E. L. Cylinder Orientation Mechanism in Block Copolymer Thin Films Upon Solvent Evaporation. *Macromolecules* **2010**, *43*, 7763–7770.
26. Kim, S. H.; Misner, M. J.; Russell, T. P. Solvent-Induced Ordering in Thin Film Diblock Copolymer/Homopolymer Mixtures. *Adv. Mater.* **2004**, *16*, 2119–2123.
27. Kim, S.; Briber, R.; Karim, A.; Jones, R. L.; Kim, H. C. Directed Self-Assembly of Thin Block Copolymer Films under Controlled Atmosphere. *Mater. Res. Soc. Symp. Proc.* **2007**, *961*, 1–6.
28. Mori, K.; Hasegawa, H.; Hashimotot, T. Ordered Structure in Block Polymer Solutions: 6. Possible Non-equilibrium Effects on Growth of Self-Assembling Structures. *Polymer* **1990**, *31*, 2368–2376.
29. Hansen, C. M. *Hansen Solubility Parameters, A User's Handbook*; CRC Press: Boca Raton, FL, 2000.
30. Bahadur, P.; Sastry, N. V. *Principles of Polymer Science*; Alpha Science International, Ltd.: Oxford, UK, 2005.
31. Elbs, H.; Krausch, G. Ellipsometric Determination of Flory–Huggins Interaction Parameters in Solution. *Polymer* **2004**, *45*, 7935–7942.
32. Helfand, E.; Tagami, Y. Theory of the Interface between Immiscible Polymers. II. *J. Chem. Phys.* **1972**, *56*, 3592–3601.
33. Hashimoto, T.; Shibayama, M.; Hiromichi, K. Ordered Structure in Block Polymer Solutions. 4. Scaling Rules on Size of Fluctuations with Block Molecular Weight, Concentration, and Temperature in Segregation and Homogeneous Regimes. *Macromolecules* **1983**, *16*, 1093–1101.
34. Jung, Y. S.; Ross, C. A. Orientation-Controlled Self-Assembled Nanolithography Using a Polystyrene–Polydimethylsiloxane Block Copolymer. *Nano Lett.* **2007**, *7*, 2046–2050.
35. Bang, J.; Kim, B. J.; Stein, G. E.; Russell, T. P.; Li, X.; Wang, J.; Kramer, E. J.; Hawker, C. J. Effect of Humidity on the Ordering of PEO-Based Copolymer Thin Films. *Macromolecules* **2007**, *40*, 7019–7025.
36. Guo, R.; Huang, H.; Chen, Y.; Gong, Y.; Du, B.; He, T. Effect of the Nature of Annealing Solvent on the Morphology of Diblock Copolymer Blend Thin Films. *Macromolecules* **2008**, *41*, 890–900.
37. Bosworth, J. K.; Paik, M. Y.; Ruiz, R.; Schwartz, E. L.; Huang, J. Q.; Ko, A. W.; Smilgies, D. M.; Black, C. T.; Ober, C. K. Control of Self-Assembly of Lithographically Patternable Block Copolymer Films. *ACS Nano* **2008**, *2*, 1396–1402.
38. Jeong, J. W.; Park, W. I.; Kim, M. J.; Ross, C. A.; Jung, Y. S. Highly Tunable Self-Assembled Nanostructures from a Poly(2-vinylpyridine-*b*-dimethylsiloxane) Block Copolymer. *Nano Lett.* **2011**, *11*, 4095–4101.
39. Zwietering, N. The Degree of Mixing in Continuous Flow Systems. *Chem. Eng. Sci.* **1959**, *11*, 1–15.
40. Cholette, A.; Cloutier, L. Mixing Efficiency Determinations for Continuous Flow Systems. *Can. J. Chem. Eng.* **1959**, *37*, 105–112.
41. Cavicchi, K. A.; Russell, T. P. Solvent Annealed Thin Films of Asymmetric Polyisoprene-Polylactide Diblock Copolymers. *Macromolecules* **2007**, *40*, 1181–1186.
42. Albert, J. N. L.; Young, W.-S.; Lewis, R. L.; Bogart, T. D.; Smith, J. R. Systematic Study on the Effect of Solvent Removal Rate on the Morphology of Solvent Vapor Annealed ABA Triblock Copolymer Thin Films. *ACS Nano* **2012**, *6*, 459–466.
43. Ginsburg, N.; Robertson, W. W.; Matsen, F. A. The Near Ultraviolet Absorption Spectrum of Toluene Vapor. *J. Chem. Phys.* **1946**, *14*, 511–517.
44. Saez, C.; Compostizo, A.; Rubio, R. G.; Colín, A. C.; Peña, M. D. Thermodynamics of Three Toluene-Containing Mixtures. Generalized van der Waals and Ising-like Models. *J. Chem. Soc. Farad. T. 1* **1986**, *82*, 1839–1852.
45. Ashcroft, S. J.; Clayton, A. D.; Shearn, R. B. Isothermal Vapor–Liquid Equilibriums for the Systems Toluene–*n*-Heptane, Toluene–Propan-2-ol, Toluene–Sulfolane, and Propan-2-ol–Sulfolane. *J. Chem. Eng. Data* **1979**, *24*, 195–199.
46. Knoll, A.; Horvat, A.; Lyakhova, K.; Krausch, G.; Sevink, G.; Zvelindovsky, A.; Magerle, R. Phase Behavior in Thin Films of Cylinder-Forming Block Copolymers. *Phys. Rev. Lett.* **2002**, *89*, 0355011–0355014.
47. Chao, C.-C.; Ho, R.-M.; Georgopanos, P.; Avgeropoulos, A.; Thomas, E. L. Silicon Oxy-carbide Nanorings from Polystyrene-*b*-Polydimethylsiloxane Diblock Copolymer Thin Films. *Soft Matter* **2010**, *6*, 3582–3587.
48. Fredrickson, G. H.; Ganesan, V.; Drolet, F. Field-Theoretic Computer Simulation Methods for Polymers and Complex Fluids. *Macromolecules* **2002**, *35*, 16–39.
49. Fredrickson, G. H. *The Equilibrium Theory of Inhomogenous Polymers*; Oxford University Press: Oxford, England, 2006.